The FASEB Journal express article 10.1096/fj.00-0550fje. Published online February 26, 2001.

Morphological aspects of spinal cord autoimmune neuroprotection: colocalization of T cells with B7-2 *(CD86)* and prevention of cyst formation

Oleg Butovsky, Ehud Hauben, and Michal Schwartz

Department of Neurobiology, The Weizmann Institute of Science, Rehovot, Israel

Corresponding author: Michal Schwartz, Department of Neurobiology, Arison Building 221 The Weizmann Institute of Science, 76100 Rehovot, Israel. E-mail: michal.schwartz@weizmann.ac.il

ABSTRACT

Autoimmune T cells directed against central nervous system associated myelin antigens were previously shown to reduce the spread of damage after axonal injury. Using morphological, morphometric, and immunocytochemical techniques, we show that, in rats with contused spinal cords, recovery after systemic treatment with such T cells is manifested by sparing of axons, including the myelin sheath, and by prevention of cyst formation. In treated cords, analysis of cellular elements revealed colocalization of T cells and B7-2, a costimulatory molecule known to be associated with activation of anti-inflammatory T cells (Th2 phenotype); some of the T cells express B7-2. It is interesting that this colocalization was restricted mainly to structures that, in the absence of the T cell treatment, developed into cystlike cavities. We conclude that interaction between myelin-specific autoimmune T cells and cellular elements in the damaged nerves, possibly mediated via microglia and in a B7-2–dependent manner, initiates a cascade that leads to secretion of a repertoire of factors that protect the neural tissue.

Key words: CNS ∘ morphology ∘ spinal cord injury ∘ secondary degeneration ∘ autoimmune neuroprotection ∘ microglia ∘ 3-dimensional reconstruction

Spinal cord injuries often have a devastating outcome in terms of neuronal degeneration, scar formation, and cyst development. The mechanisms underlying the occurrence of these processes, some of which develop over a long period, are not fully understood. Accumulating evidence suggests, however, that the progressive degeneration of axons and cell bodies that escaped the primary injury is caused by a toxic increase in glutamate and free radicals, alterations in ion composition, and other hostile changes in the nerve's extracellular environment resulting from the active degeneration of initially injured neurons (1–8).

Immune cells, as well as the molecules associated with them, are widely thought to play contradictory roles in recovery from spinal cord injury, as in recovery from injuries of the central

nervous system (CNS) in general. For example, when anti-inflammatory compounds are administered within a few hours after injury, they appear to have a beneficial effect (9–18). Thereafter, however, they seem to be ineffective, and at least in terms of regeneration possibly even harmful (19–22).

Experiments in recent years strongly suggest that recovery of the injured CNS may, as in other tissues, require active immune cell participation. For example, the recruitment and activation of macrophages at the site of injury, a crucial step in the successful regeneration of the peripheral nervous system (PNS) (23), is both delayed and limited in the CNS, which possibly accounts—at least in part—for the failure of injured nerves to regenerate (24). Implantation of PNS-activated macrophages into the transected optic nerves or spinal cords of rats induces axonal regrowth and partial functional recovery (25, 26). It therefore seems that the active involvement of stimulated macrophages is essential for axonal regrowth. Moreover, it was recently shown in our laboratory that T cells specific to myelin-associated antigens protect against secondary degeneration in two rat CNS models, the crush-injured optic nerve (27, 28) and the contused spinal cord (29, 30). Furthermore, although systemic injection of T cells in these models was followed by T cell accumulation at the site of injury, only those T cells directed specifically against CNS myelin-associated self-antigens were neuroprotective. The beneficial effect of these T cells was demonstrated and confirmed by morphological, physiological, and imaging criteria. Systemic treatment with autoimmune T cells specific to myelin basic protein (MBP) promoted recovery of the partially injured spinal cord, manifested by the sparing of neural tissue that would otherwise have undergone secondary degeneration (29, 30).

The present study was undertaken to characterize the interrelationships between T cells, macrophages/microglia, expression of costimulatory molecules such as B7-2, and resident cells within the damaged tissue at various times after injury. We also examined whether the systemic injection of anti-MBP T cells (T_{MPB}) has a beneficial effect on any other injury-related destructive events, such as cyst formation. Our results indicate that the recovery induced by these autoimmune T cells is manifested not only by tissue preservation but also by prevention of cyst formation. Moreover, in the recovered rats we observed colocalization of B7-2–expressing cells and T_{MPB} in areas, which, in the absence of T_{MPB} treatment, would have shown cyst development.

MATERIALS AND METHODS

Animals

Inbred adult female Lewis rats (10 12 wks old, 200 250 g) were supplied by the Animal Breeding Center of the Weizmann Institute of Science. The rats were housed in a light- and temperature-controlled room and matched for age in each experiment. Animals were handled according to the regulations formulated by the Institutional Animal Care and Use Committee.

Antigen

MBP was prepared from the spinal cords of guinea pigs or purchased from Sigma (St. Louis, Mo.).

Spinal cord contusion

Forty-eight female rats were divided into three groups and examined 7, 14, 28 days or 21 wks after injury. Rats in the first group (n=18) were subjected to spinal cord contusion as described below, and immediately afterwards were injected intraperitoneally with 10^7 T_{MBP}. Rats in a second group ("sham-operated", n=12) were injected with 10^7 T_{MBP} after being subjected to laminectomy without spinal cord contusion. Rats in the third group (n=18, controls) were injured and injected with phosphate-buffered saline (PBS).

Prior to spinal cord contusion, the rats were deeply anesthetized (ketamine 40 mg/kg, xylazine 10 mg/kg). Their spinal cords were exposed by laminectomy at the level of T8 T9, and the rats were placed on a heating pad set at 37.5 C. One hour after induction of anesthesia, a 10 g rod was dropped onto the laminectomized cord from a height of 50 mm. The NYU impactor was used to displace the rod over a distance of 0.9 mm (moderate injury level) for 23 ms, which caused immediate and complete hind-limb paralysis. Within 1 h of contusion the rats were injected intraperitoneally, on a random basis, with 10^7 T_{MBP} or with PBS. Bladder expression was carried out manually at least twice a day (particularly during the first 48 h after injury, when it was done up to three times a day). The rats were carefully monitored for evidence of urinary tract infection or any other sign of systemic disease. During the first week after contusion and in any case of hematuria thereafter, they received a course of sulfamethoxazole (400 mg/ml) and trimethoprim (8 mg/ml) (Resprim, Teva Laboratories, Israel), administered orally with a tuberculin syringe (0.3 ml of solution per day). Daily inspection included examination of the laminectomy site for evidence of infection and assessment of the hind limbs for signs of autophagia or pressure.

Evaluation of recovery

Observers, blinded to the treatment received by the rats, scored behavioral recovery on a scale of 0 (complete paralysis) to 21 (complete mobility) (31–33). Approximately twice a week the locomotion activities of the trunk, tail, and hind limbs of all rats were evaluated in an open field by placing each rat for 4 min in the center of a circular enclosure made of molded plastic with a smooth, nonslip floor (90 cm diameter, 7 cm wall height). Prior to each evaluation, rats were carefully examined for perennial infection, wounds in the hind limbs, or tail and foot autophagia.

T cell lines

T cell lines were generated from draining lymph node cells obtained from Lewis rats immunized with MBP, as described (34, 35). The antigen was dissolved in PBS (1 mg/ml) and emulsified with an equal volume of incomplete Freund's adjuvant (Difco Laboratories, Detroit, Mich.) supplemented with 4 mg/ml *Mycobacterium tuberculosis* (Difco). Ten days after the antigen was injected into the rats' hind footpads in 0.1 ml of the emulsion, the rats were killed; draining lymph nodes were surgically removed and dissociated. The cells were washed and activated with the antigen (10 g/ml) in proliferation medium containing Dulbecco's modified Eagle's medium (DMEM) supplemented with L-glutamine (2 mM), 2-mercaptoethanol (5 10^{-5} M), sodium pyruvate (1 mM), penicillin (100 IU/ml), streptomycin (100 g/ml), nonessential amino acids, and autologous rat serum 1% (volume/volume). After incubation for 72 h at 37 C, 90% relative

humidity and 7% CO_2, the cells were transferred to propagation medium consisting of DMEM, L-glutamine, 2-mercaptoethanol, sodium pyruvate, nonessential amino acids and antibiotics, in the same concentrations as above, as well as 10% fetal calf serum (volume/volume) and 10% T cell growth factor derived from the supernatant of concanavalin A-stimulated spleen cells. The cells were grown in propagation medium for 4 to 10 days before being restimulated with their antigen (10 g/ml) in the presence of irradiated thymus cells (10^7 cells/ml; 2000 rad) in proliferation medium. The T cell lines were expanded by repeated stimulation and propagation.

Tissue processing

Prior to longitudinal sectioning of the spinal cord, each rat was perfused intracardially with 200 ml (on average) of cold PBS followed by 200 ml of paraformaldehyde (4% prepared in 0.1 M phosphate buffer with glucose 5%). Their spinal cords were removed, postfixed overnight, briefly rinsed in PBS, and transferred to sucrose 30% for cryoprotection for at least 3 days. All procedures were carried out at 4 C. A 30-mm block of the spinal cord, with the injury site at the center, was excised embedded in Tissue-Tek (Miles, Ind.) and placed in liquid nitrogen. Frozen longitudinal 30-mm blocks were sectioned (20 m) on a cryostat, collected onto gelatin-coated slides, and dried at room temperature.

For axial section, the procedures were the same except that cryoprotection was omitted and the spinal cords were postfixed for 72 h. An excised 20-mm block of the spinal cord, with the injury site at the center, was then sequentially divided in the transverse plane into three separate 6-mm fragments and embedded in a paraffin block. The blocks were serially sectioned (4 m) in the transverse plane, and eight sections from each fragment were taken at intervals of 800 m for immunohistochemistry, histology, and 3-dimensional (3D) reconstruction analysis.

Microglia and T_{MBP} cells coculturing

Microglia cells were purified from the cerebral cortex of newborn (day 0) Lewis rat as previously described (36). The cells were cultured as mixed glia culture for 7 days. Microglia were then separated from other glia cells by shaking for 6 h at 37 C. The cells were then seeded on poly-d-lysine (20 g/ml) (Sigma-Aldrich, Israel) coated coverslips in 24 wells (10^5 cells/1 ml/well). The cells were incubated in 37 C, 5% CO_2 for 3 days before T_{MBP}-activated cells were added. Both microglia and T_{MBP}-activated cells (2 10^3, 2 10^4, 2 10^5 cells/1 ml/well) were cocultured in the presence or without of anti-rat IFN- neutralizing antibody (1 g/ml) (R&D Systems, Minneapolis, Minn.) in RPMI-1640 medium (Sigma-Aldrich, Israel) containing 10% FCS, 50 M 2-mercaptoethanol (Sigma), 1 mM sodium pyruvate, 2 mM L-glutamine, 100 IU/ml penicillin, and 100 g/ml streptomycin for 24 h. Thereafter, the microglia cells were prepared for immunocytochemistry.

Immunohistochemistry

Tissue sections were fixed in absolute ethanol for 10 min at room temperature, washed twice in double-distilled water, and incubated for 3 min with 0.5% Tween-20 (Sigma). To increase permeability and reduce nonspecific staining, the sections were blocked with a solution containing 4% normal fetal calf serum and 0.1% Triton X-100 (Sigma). Incubation with the

primary antibody diluted in blocking solution was followed by incubation with the appropriate secondary antibodies in blocking solution. The primary antibodies were the monoclonal antibodies ED-1 (1:250; Serotec, Oxford, U.K.) for labeling of activated macrophages and microglia, anti-rat T cell receptor (TCR) for detection of T cells (37), anti-B7-2 (CD86, 1:10, Pharmingen, San Diego, Calif.) for labeling of costimulatory molecules, anti-glial fibrillary acid protein (GFAP, diluted 1:100; NeoMarkers, Fremont, Calif.) for identification of astrocytes, and antineurofilament (NF, a mixture of 68 kDa and 200 kDa, diluted 1:50; Novacastra Laboratories, Newcastle upon Tyne U.K.) for identification of nerve fibers. Each of these antibodies was applied to the tissue sections for 1 h at room temperature in a humidified chamber. Sections were rinsed three times with Tris-buffered saline (0.05% Tween-20 in PBS) and then incubated with fluorescein-conjugated secondary antibody (Alexa-488 or Alexa-546, diluted 1:200 [Molecular Probes, Eugene, Ore.] or Cy3-1:200 [Jackson ImmunoResearch, West Grove, Pa.]) for 1 h at room temperature. Control sections (not treated with primary antibody) were used to distinguish specific staining from nonspecific antibody binding and/or autofluorescent components of injured areas. To reduce or eliminate autofluorescence emanating from the massive presence of lipofuscin in neural tissues, the sections were washed well and treated for 8 min with a solution of 0.3% Sudan Black B (SBB) (38), (Merck, Darmstadt, Germany) in 70% ethanol. If overstained, the sections were dipped in clean 70% ethanol until staining was satisfactory. They were then mounted with antifading oil and coverslips and examined under a Zeiss laser-scanning confocal microscope (LSM510) and/or a Zeiss Axioplane 100 fluorescence light microscope. The results were analyzed by an observer who was blinded to the treatment received by the rats

For 3D reconstruction of cyst cavitation, glial scar formation and neurofilament preservation, and for measurement of the lesion volume, 21 serial transverse slices were analyzed by SurfDriver 3.5 software. First, the slice boundaries were extracted as the sole feature used in the 3D model. This extraction is usually done manually, because such segmentation cannot be achieved with sufficient accuracy by using the SurfDriver software. The second step was to construct the main 3D-wireframe model. This step is done by linking the boundary images to each other and using small triangular objects to approximate curved surfaces. Finally, by assigning material texture to the approximated surfaces and using pseudocoloring, shading, and opacity functions, we can visualize information that is located inside other 3D objects (39). This application has proved extremely useful, especially for reconstruction of cystic cavitation, as it allows the internal cyst and any morphological changes to be presented in combination with the external outline of the spinal cord.

Statistical evaluation

Estimation was performed by using INSTAT software; data sets were compared by using one-way ANOVA or Student's two-tailed test of significance.

RESULTS

Dynamics of T cell recruitment, macrophage recruitment and/or microglia activation

showed a high degree of preservation, and if any cysts were present they were very small (Fig. 3, A1). Staining for GFAP showed a wider gap at the lesion site in longitudinal sections from the spinal cords of the PBS-treated controls (Fig. 3, C2) than in corresponding sections from the T_{MBP}-treated group (Fig. 3, C1). Staining for NF in the PBS-treated cords (Fig. 3, B2) showed a large gap in the continuity of NF staining across the lesion site, with minimal staining distal to the lesion. In the T_{MBP}-treated cords (Fig. 3, B1), however, there were a sizeable number of well-organized nerve fibers across the lesion site, pointing to the rescue of viable tissue rather than the formation of newly growing and newly organized neural tissue.

Differences in T cell distribution and T cell accumulation in the spinal cords of T_{MBP}-treated and PBS-treated rats, at the indicated time points, are shown in Figure 4. The time-related changes of the size of the site of the lesion delineated by GFAP staining in the T_{MBP}-treated but not in the PBS-treated rats, are quantified in Figure 5.

Immunocytochemical and histological analysis of the lesion site

Serial axial sections of spinal cords from T_{MBP}-treated and PBS-treated rats were stained for NF (Fig. 6, A and B, respectively) and GFAP (Fig. 6, C and D, respectively) and examined by high-resolution scanning confocal microscopy. Sections from a T_{MBP}-treated rat relative to those of parallel sections of PBS-treated rats showed lower intensity of GFAP staining (Fig. 6, C vs. D), smaller cystic structures, and lower degree of loss of neural tissue (Fig. 6, A vs. B).

Luxol staining for myelin (Fig. 7A) revealed an abundance of myelinated axons in the spinal cords of the T_{MBP}-treated rats. Staining with hematoxylin and eosin (H&E) revealed evidence of tissue organization (Fig. 7B). In contrast, Luxol-stained sections from control rats (Fig. 7C) showed complete loss of myelin at the site of the lesion, with myelin staining visible only in the dorsal and ventral roots. Large necrotic areas and a fibrillary tissue matrix were seen within the lesion (Fig. 7D). Specificity of Luxol staining for myelin is shown under high magnification in Figure 7E. Sections taken from the same area were also stained for NF (Fig. 7F). GFAP immunoreactivity was less evident in sections from T_{MBP}-treated rats than in sections from PBS-treated controls. In the latter, the site of injury was filled with a dense meshwork of GFAP-immunoreactive fibers (Fig. 7I), whereas in sections from T_{MBP}-treated rats, only activated astrocytes were seen (Fig. 7H). Note the appearance of neuronal cell bodies in the ventral horn of T_{MBP}-treated spinal cords (Fig. 7G—boxed area in A at high magnification), whereas in the control sections they were hardly noticeable (Fig. 7J—boxed area in C at high magnification).

3-dimensional reconstruction

The 3D model used in this study, known as a surface representation model (40–45), is based on information extracted from a series of axial spinal cord sections stained for NF and GFAP (Fig. 6). This model allows reconstruction of external and internal surfaces, enabling visualization of cyst formation, distribution of gliosis, and preservation of neurofilaments. The result is a set of curved, closed surfaces that define the shape and topological characteristics of the reconstructed spinal cord. The internal volumes of the cysts in the T_{MBP}-treated and control rats were calculated and compared by SurfDriver software. Treatment with anti-MBP T cells resulted in a significant (5.2-fold) decrease in cyst volume relative to controls (Fig. 8). This finding appears to

confirm our contention that treatment with the anti-MBP T cells promotes rescue and protection of undamaged neurons, thereby reducing the lateral and longitudinal spread of damage.

Spatial relationship between B7-2 expression and T cells

As shown above, in the spinal cords of T_{MBP}-treated rats the expression of B7-2 was increased (Fig. 1). To determine the cellular distribution of B7-2, we further analyzed sections taken 14 and 28 days after injury and treatment (Figs. 9 and 10, respectively). The fields represented in these figures were scanned by confocal microscopy with superimposed bright-field. In sections from T_{MBP}-treated rats, B7-2 expression appeared to be limited to the putative precyst structures and to be mainly colocalized with T cells (Fig. 9 A1, A2). In contrast, in the control sections, B7-2 immunoreactivity was hardly detected (Fig. 9F), and only a few T cells were detected at the margins of the precystlike structures (Fig. 9 D, E). Double labeling for T cell receptor and for B7-2 was applied to verify that B7-2 is associated with T cells and not only colocalized with them in terms of the area. (Fig. 9 G1–G6). Thus, Figure 9 G1 shows staining for B7-2 and Figure 9 G2 shows staining for TCR on the same cells. Figure 9 G3 shows the same cell stained for both. Because the availability of the primary antibodies used here was such that both anti-B7-2 antibodies and the antibodies recognizing T cell receptor were both raised in the same species, the secondary antibodies were directed against the same species but differently tagged. Figure 9 G4–G6 shows the control for the staining when the first antibody was outlined (see Materials and Methods). By 28 days postinjury (Fig. 10), this pattern had changed: In the sections from T_{MBP}-

demonstrated that systemic injection of autoimmune T cells immediately after severe contusion (T8 T9) of the rat spinal cord promotes recovery of locomotion activity, a fivefold increase in the number of intact axons descending from the red nucleus, and a significant increase in the mass of spared spinal cord tissue (29, 30). The main conclusion was that the effect of these autoimmune T cells on recovery results from the protection of neurons whose axons had escaped the primary lesion. The object of the present study was to characterize the cellular elements of the protected tissue and to determine whether the autoimmune T cells make a further contribution to recovery, possibly by reducing glial scarring and cyst formation.

In humans, spinal cyst formation, or syringomyelia, is a condition characterized by the presence in the spinal cord of longitudinal cavities lined by dense gliogenous tissue and is often associated with progressive myelopathy (46–49). We show here that T_{MBP} can prevent glial scarring and the development of syringomyelia; that is, fluid-filled cavities or cysts that interrupt neural pathways in the central part of the spinal cord. We further show that the presence of T_{MBP} appears to be colocalized with up-regulated expression of B7-2 costimulatory molecules within the site of the lesion and caudally to it. The increased expression of B7-2 is associated, at least in part, with the accumulated T cells (endogenous or adaptively transferred). These findings suggest that the induction of B7-2 expression plays an important role in preserving neuronal tissue and may be associated with the neuroprotective phenotype of T_{MBP}.

Studies from our laboratory have strongly suggested that in the injured CNS, accumulation of

Our present results indicate that the recovery induced by autoimmune T cells is manifested not only by tissue preservation but also by the prevention of cyst formation. Neural tissues from the T_{MBP}-treated rats were found to be well preserved, with only small cysts seen at the site of injury. In contrast, in PBS-treated controls there was severe damage to the gray matter and enlarged cystlike structures were seen. Furthermore, in the T_{MBP}-treated rats, the accumulating T cells were found to be colocalized with the expression of costimulatory B7-2 molecules on microglia, and to be located adjacent to structures, which, in the absence of T cells, developed into cysts. The dramatic increase in B7-2 expression was associated with an immune response that was neuroprotective in its effect. These observations prompt us to suggest that resident macrophages (microglia) might be activated by their interaction with activated T cells, leading to axonal regrowth and partial functional recovery. Signals derived from preactivated $CD4^+$ T cells are thought to be crucial for microglia activation (60–63). *In vitro*, T_{MBP}-activated cells were found to induce the expression of costimulatory molecules on cultured rat microglia, possibly via IFN- activity. The up-regulation of B7-2 is possibly leading to an enhanced ability of microglia to support antigen-dependent T cell activation. Recently it was shown that antigen-specific interactions between microglia and Th1 cells *ex vivo* induce the expression of MHC class II and adhesion/costimulatory molecules, resulting in activation of Th1 or naive T cells but not of Th2 (64, 65). Those observations are in line with our *in vivo* and *in vitro* findings that interactions between activated T_{MBP} and resting microglia can stimulate the expression of B7-2 costimulatory molecules on microglia. These findings suggest that infiltration of the CNS by preactivated T cells may cause resident microglia to mature into competent antigen presenting cells that can

3. Yoles, E., Zalish, M., Lavie, V., Duvdevani, R., Ben-Bassat, S., and Schwartz, M. (1992) GM1 reduces injury-induced metabolic deficits and degeneration in the rat optic nerve. *Invest. Ophthalmol. Vis. Sci.* **33,** 3586–3591

4. Faden, A.I. (1993) Experimental neurobiology of central nervous system trauma. *Crit. Rev. Neurobiol.* **7,** 175–186

5. Lynch, D.R., and Dawson, T.M. (1994) Secondary mechanisms in neuronal trauma [see comments]. *Curr. Opin. Neurol.* **7,** 510–516

6. Povlishock, J.T., and Jenkins, L.W. (1995) Are the pathobiological changes evoked by traumatic brain injury immediate and irreversible? *Brain Pathol.* **5,** 415–426

7. Bazan, N.G., Rodriguez de Turco, E.B., and Allan, G. (1995) Mediators of injury in neurotrauma: intracellular signal transduction and gene expression. *J. Neurotrauma* **12,** 791–814

8. Yoles, E., and Schwartz, M. (1998) Degeneration of spared axons following partial white matter lesion: implications for optic nerve neuropathies. *Exp. Neurol.* **153,** 1–7

within the brain: modulation of tumor necrosis factor-alpha production by human astrocytic cells. *Neuroimmunomodulation* **4,** 37–41

16. Bethea, J.R., Nagashima, H., Acosta, M.C., Briceno, C., Gomez, F., Marcillo, A.E., Loor, K., Green, J., and Dietrich, W.D. (1999) Systemically administered interleukin-10 reduces tumor necrosis factor- alpha production and significantly improves functional recovery following traumatic spinal cord injury in rats. *J. Neurotrauma* **16,** 851–863

17. Yan, P., Xu, J., Li, Q., Chen, S., Kim, G.M., Hsu, C.Y., and Xu, X.M. (1999) Glucocorticoid receptor expression in the spinal cord after traumatic injury in adult rats. *J. Neurosci* **19,** 9355–9363

18. Lu, J., Ashwell, K.W., and Waite, P. (2000) Advances in secondary spinal cord injury: role of apoptosis. *Spine* **25,** 1859–1866

19. Bracken, M.B. (1991) Treatment of acute spinal cord injury with methylprednisolone: results of a multicenter, randomized clinical trial. *J. Neurotrauma* **8 Suppl 1,** S47–50; discussion S51–42

20. Hall, E.D., Yonkers, P.A., Taylor, B.M., and Sun, F.F. (1995) Lack of effect of postinjury treatment with methylprednisolone or tirilazad mesylate on the increase in eicosanoid

Implantation of stimulated homologous macrophages results in partial recovery of paraplegic rats. *Nat. Med.* **4,** 814–821

27. Moalem, G., Leibowitz-Amit, R., Yoles, E., Mor, F., Cohen, I.R., and Schwartz, M. (1999) Autoimmune T cells protect neurons from secondary degeneration after central nervous system axotomy. *Nat. Med.* **5,** 49–55

28. Kipnis, J., Yoles, E., Porat, Z., Cohen, A., Mor, F., Sela, M., Cohen, I.R., and Schwartz, M. (2000) T cell immunity to copolymer 1 confers neuroprotection on the damaged optic nerve: possible therapy for optic neuropathies. *Proc. Natl. Acad. Sci. USA* **97,** 7446–7451

29. Hauben, E., Nevo, U., Yoles, E., Moalem, G., Agranov, E., Mor, F., Akselrod, S., Neeman, M., Cohen, I.R., and Schwartz, M. (2000) Autoimmune T cells as potential neuroprotective therapy for spinal cord injury [letter]. *Lancet* **355,** 286–287

30. Hauben, E., Butovsky, O., Nevo, U., Yoles, E., Moalem, G., Agranov, E., Mor, F., Leibowitz-Amit, R., Pevsner, E., Akselrod, S., Neeman, M., Cohen, I.R., and Schwartz, M. (2000) Passive or active immunization with myelin basic protein promotes recovery from spinal cord contusion. *J. Neurosci.* **20,** 6421–6430

31. Basso, D.M., Beattie, M.S., and Bresnahan, J.C. (1995) A sensitive and reliable

induces T cell activation. Differential reactivity with subsets of immature and mature T lymphocytes. *J. Exp. Med.* **169,** 73–86

38. Romijn, H.J., van Uum, J.F., Breedijk, I., Emmering, J., Radu, I., and Pool, C.W. (1999) Double immunolabeling of neuropeptides in the human hypothalamus as analyzed by confocal laser scanning fluorescence microscopy. *J. Histochem. Cytochem.* **47,** 229–236

39. Moriarty, L.J., Duerstock, B.S., Bajaj, C.L., Lin, K., and Borgens, R.B. (1998) Two- and three-dimensional computer graphic evaluation of the subacute spinal cord injury. *J. Neurol. Sci.* **155,** 121–137

40. Winder, J., Cooke, R.S., Gray, J., Fannin, T., and Fegan, T. (1999) Medical rapid prototyping and 3D CT in the manufacture of custom made cranial titanium plates. *J. Med. Eng. Technol.* **23,** 26–28

41. Janssen, T., Bohnke, F., and Steinhoff, H.J. (1987) [Spatial representation of basilar membrane movement with 3D computer graphics]. *Hno* **35,** 302–309

42. Borodkin, M.J., and Thompson, J.T. (1992) Retinal cartography. An analysis of two-dimensional and three-dimensional mapping of the retina. *Retina* **12,** 273–280

49. Stoodley, M.A., Gutschmidt, B., and Jones, N.R. (1999) Cerebrospinal fluid flow in an animal model of noncommunicating syringomyelia. *Neurosurgery* **44,** 1065–1075; discussion 1075–1066

50. Hirschberg, D.L., Moalem, G., He, J., Mor, F., Cohen, I.R., and Schwartz, M. (1998) Accumulation of passively transferred primed T cells independently of their antigen specificity following central nervous system trauma. *J. Neuroimmunol.* **89,** 88–96

51. Young, W. (1996) Spinal cord regeneration [comment]. *Science* **273,** 451

52. Yoles, E., and Schwartz, M. (1998) Potential neuroprotective therapy for glaucomatous optic neuropathy. *Surv. Ophthalmol.* **42,** 367–372

53. Schwartz, M., Moalem, G., Leibowitz-Amit, R., and Cohen, I.R. (1999) Innate and adaptive immune responses can be beneficial for CNS repair. *Trends Neurosci.* **22,** 295–299

54. Moalem, G., Yoles, E., Leibowitz-Amit, R., Muller-Gilor, S., Mor, F., Cohen, I.R., and Schwartz, M. (2000) Autoimmune T cells retard the loss of function in injured rat optic nerves [In Process Citation]. *J. Neuroimmunol* **106,** 189–197

61. Matyszak, M.K., Denis-Donini, S., Citterio, S., Longhi, R., Granucci, F., and Ricciardi-Castagnoli, P. (1999) Microglia induce myelin basic protein-specific T cell anergy or T cell activation, according to their state of activation. *Eur. J. Immunol.* **29,** 3063–3076

62. Aloisi, F., Penna, G., Polazzi, E., Minghetti, L., and Adorini, L. (1999) CD40-CD154 interaction and IFN-gamma are required for IL-12 but not prostaglandin E2 secretion by microglia during antigen presentation to Th1 cells. *J. Immunol.* **162,** 1384–1391

63. Aloisi, F., Serafini, B., and Adorini, L. (2000) Glia-T cell dialogue. *J. Neuroimmunol.* **107,** 111–117

64. Aloisi, F., Ria, F., Penna, G., and Adorini, L. (1998) Microglia are more efficient than astrocytes in antigen processing and in Th1 but not Th2 cell activation. *J. Immunol.* **160,** 4671–4680

65. Aloisi, F., De Simone, R., Columba-Cabezas, S., Penna, G., and Adorini, L. (2000) Functional maturation of adult mouse resting microglia into an APC is promoted by granulocyte-macrophage colony-stimulating factor and interaction with Th1 cells. *J. Immunol.* **164,** 1705–1712

66. Popovich, P.G., Wei, P., and Stokes, B.T. (1997) Cellular inflammatory response after

Fig. 1

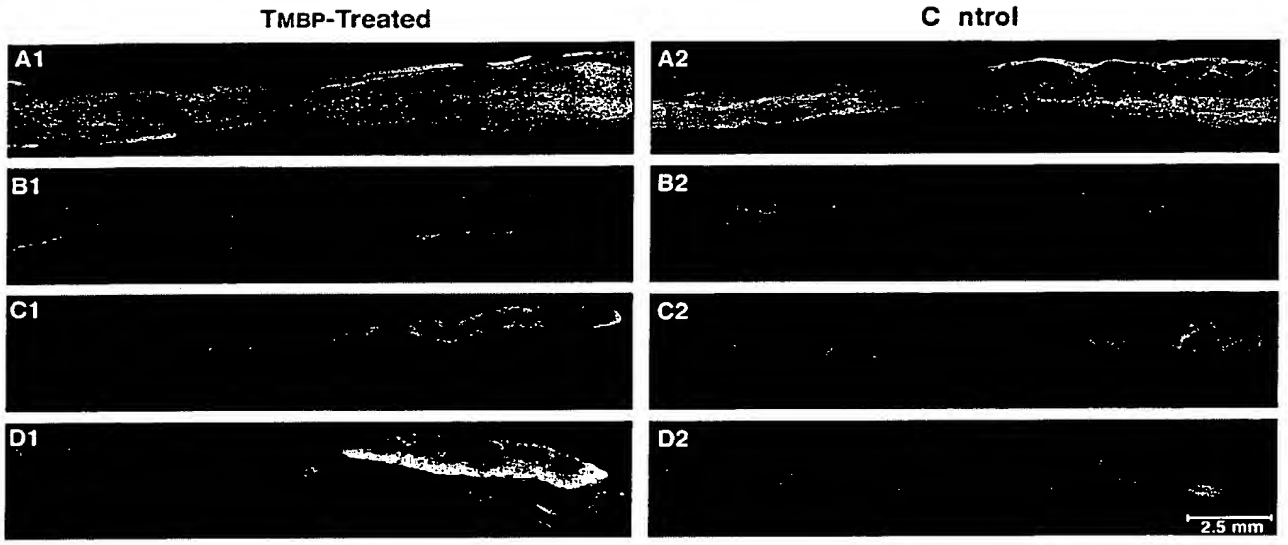

Figure 1. Montages of fluorescence micrographs of longitudinal mid-sagittal sections of the spinal cord of a T_{MBP}-treated rat and a PBS-treated control, 14 days after contusion. Micrographs are from T_{MBP}-treated rats (A1–D1) and PBS-treated controls (A2–D2). (A1, A2) Fluorescence micrographs stained for neurofilaments (NF). The gap between the

Fig. 2

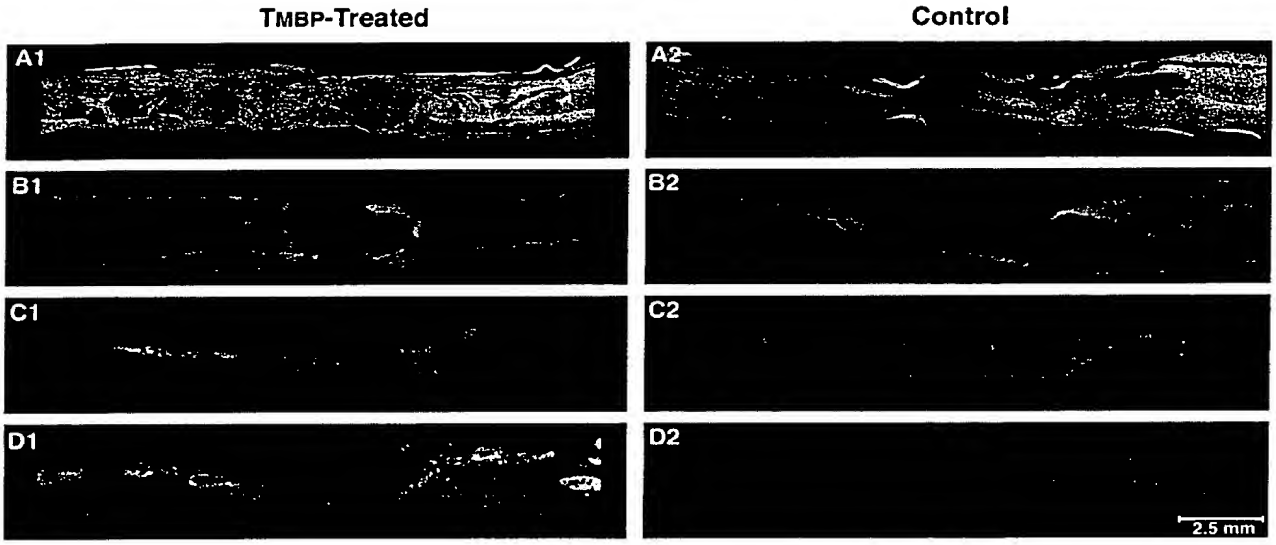

Figure 2. Montages of fluorescence micrographs of longitudinal mid-sagittal sections of the spinal cord of a T_{MBP}-treated rat and a PBS-treated control, 28 days after contusion. Micrographs are from T_{MBP}-treated rats **(A1–D1)** and PBS-treated controls **(A2–D2)**. **(A1, A2)** Fluorescence micrographs stained for neurofilaments (NF). Note the large gap (disrupted axons) in the spinal cord sections from a PBS-treated rat **(A2)** compared with those from a T_{MBP}-treated rat **(A1)**. **(B1, B2)** The lesion site in the T_{MBP}-treated rat shows massive invasion of GFAP-immunoreactive glial fibers. In contrast, in the PBS-treated rat, intense labeling at the margins of the lesion surrounds a large gap. **(C1, C2)** Labeled macrophages and microglia. There are no evident differences between T_{MBP}-treated and PBS-treated control rats. **(D1, D2)** Fluorescence micrographs show staining for B7-2. The B7-2-expressing cells are fewer in number than on the 14th day after injury (Fig. 1) and are dispersed both rostrally and caudally in the gray matter of the T_{MBP}-treated rat. No B7-2-labeled cells were detected in the PBS-treated rat.

Fig. 3

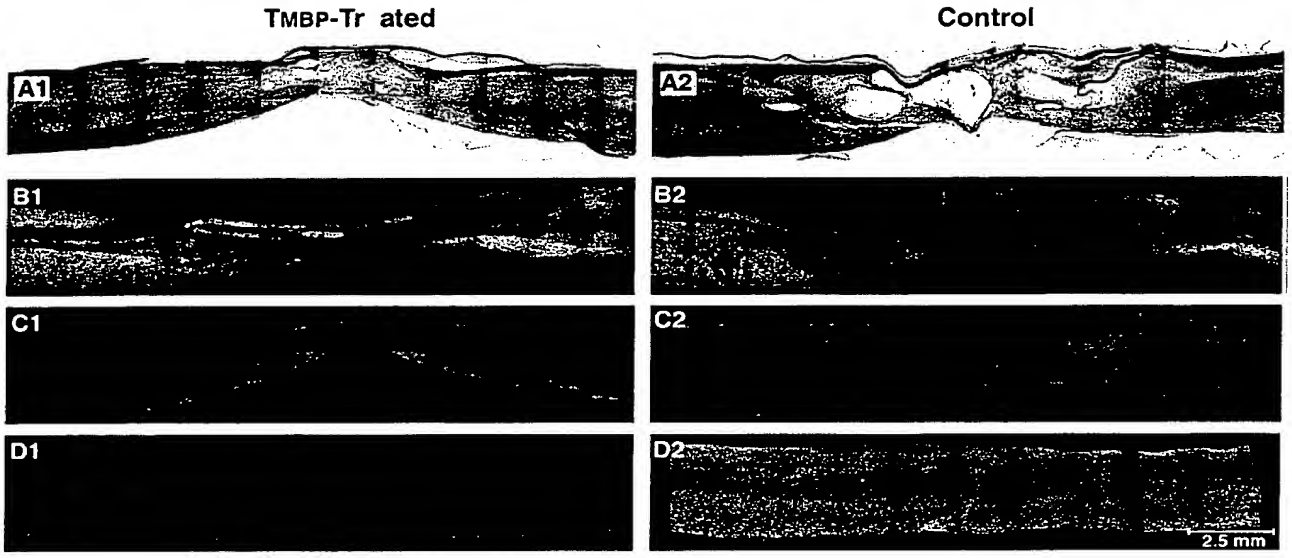

Figure 3. Montages of fluorescence and bright-field micrographs of longitudinal mid-sagittal sections of the spinal c rd of a T_{MBP}-treated rat and a PBS-treated control, 21 wks after contusion. Micrographs are from T_{MBP}-treated rats

Fig. 4

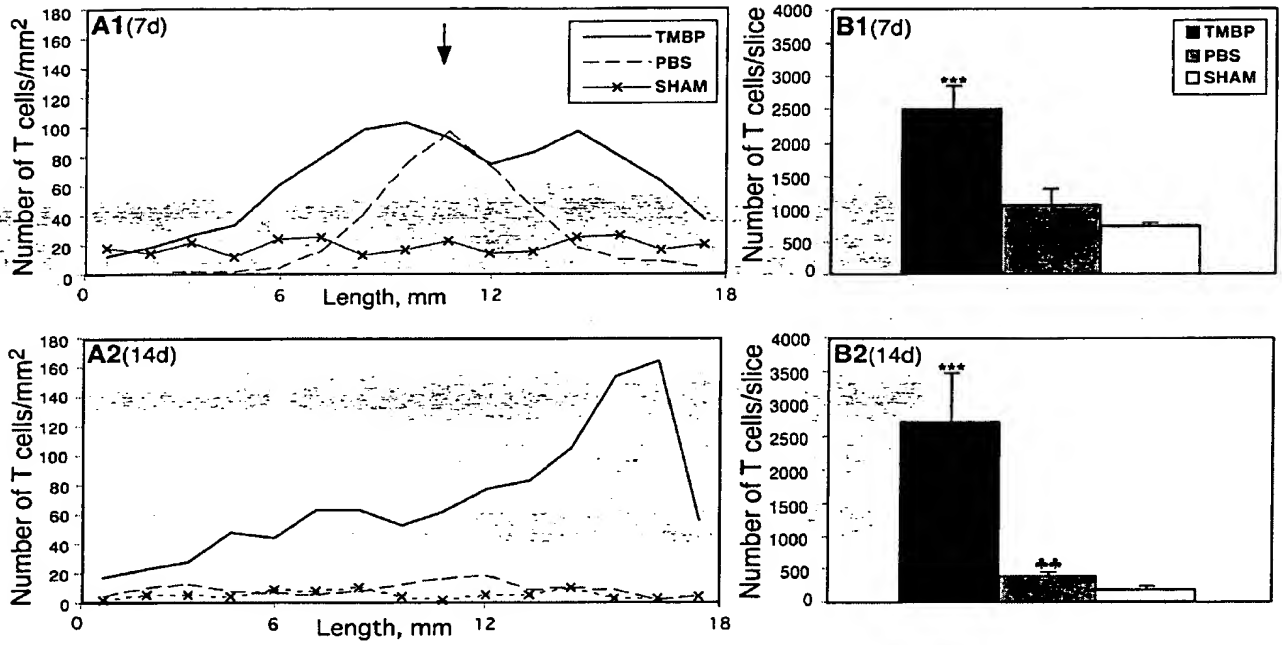
A1(7d)
TMBP
PBS
SHAM
Number of T cells/mm2
Length, mm
B1(7d)
Number of T cells/slice
***
A2(14d)
B2(14d)
**

Fig. 5

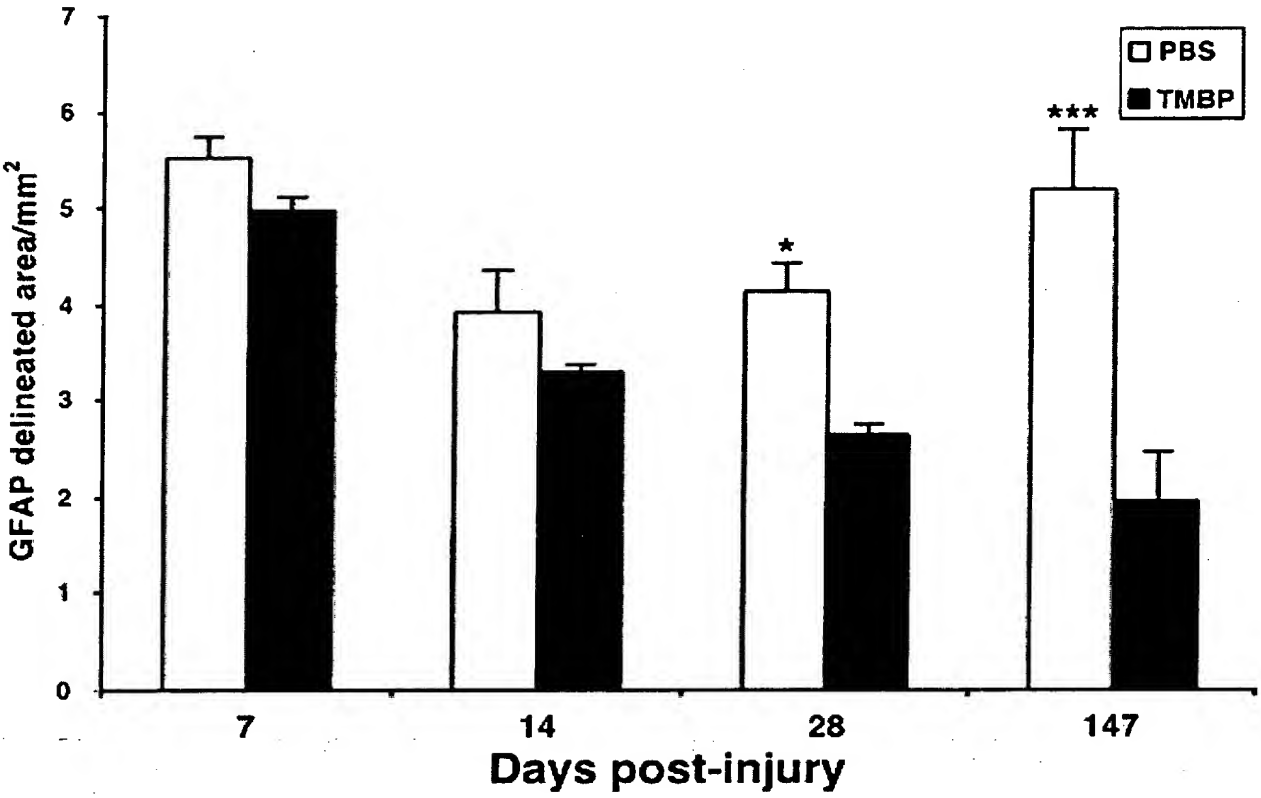

Figure 5. Estimation of the area of the lesion delineated by GFAP staining. Graphic comparison and statistical analysis of astrocytes-free areas (SE, in mm^2) in T_{MBP}-treated (n=4) and PBS-treated rats (n=4). The data show the reduction in GFAP-free area in T_{MBP}-treated rat's 21 wks after injury; that is, after a steady state was reached. On the 7th and 14th days after injury, there was no significant difference in GFAP-free area between the T_{MBP}-treated and the PBS-treated groups. Differences were significant between the two groups at 28 days ($p<0.05$) and at 21 wks ($p<0.001$) post-injury. Note the reduction in lesioned area in the spinal cords of T_{MBP}-treated rat and the lack of change in the PBS-treated control.

Fig. 6

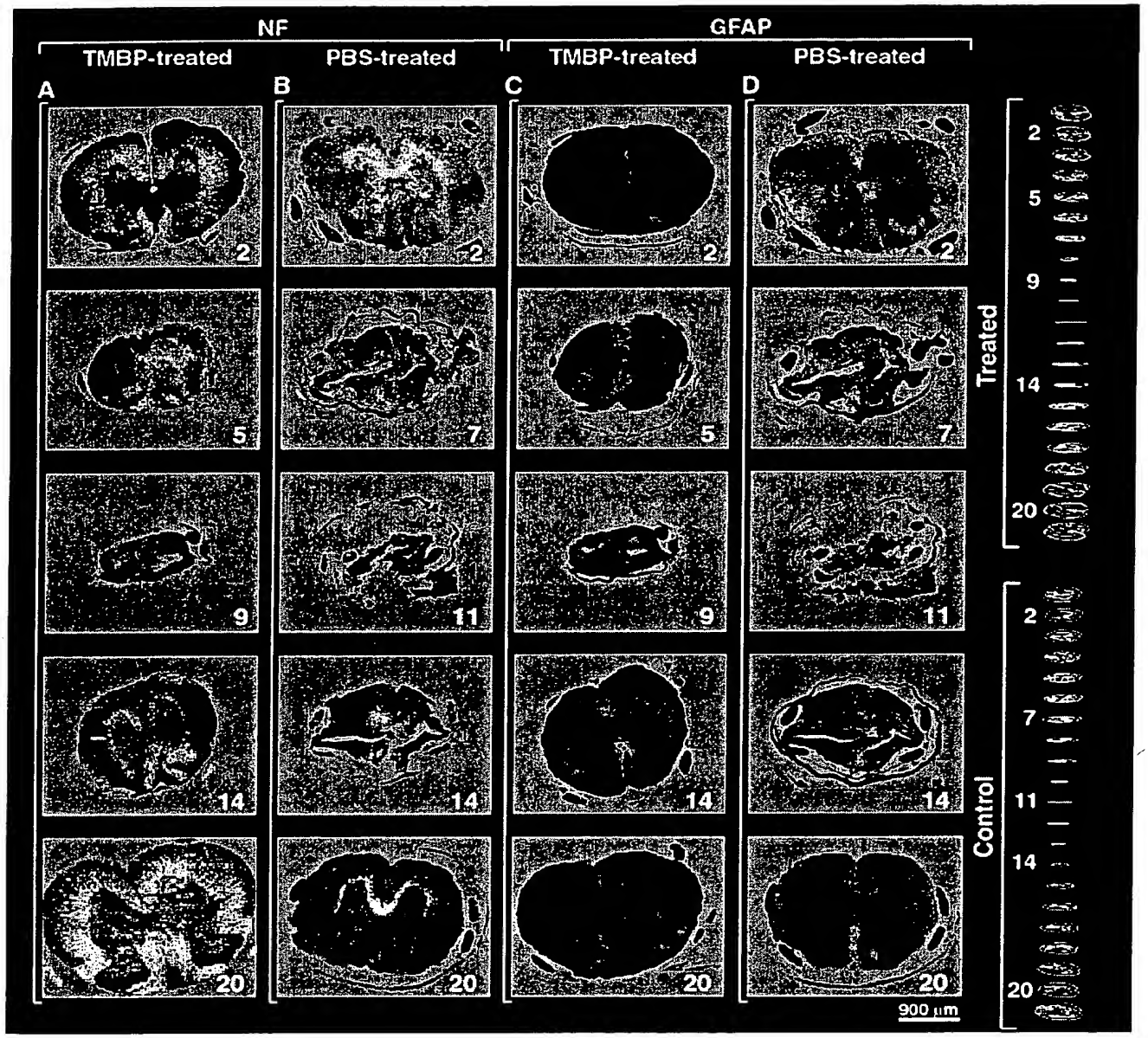

Figure 6. Serial axial sections of spinal cord stained for NF and GFAP. Sections were scanned by confocal microscope with superimposed light transmission to show the tissue texture. Columns **(A, C)** Sections from a T_{MBP}-treated rat stained for NF (green) and GFAP (red). Columns **(B, D)** Sections from a PBS-treated rat stained for NF (green) and GFAP (red). The numbers on each section represent the slice number in the spinal cord (from rostral to caudal, from up to down). NF-labeled and GFAP-labeled slices with the same number are from the same position. The wire frame is shown on the right.

Fig. 7

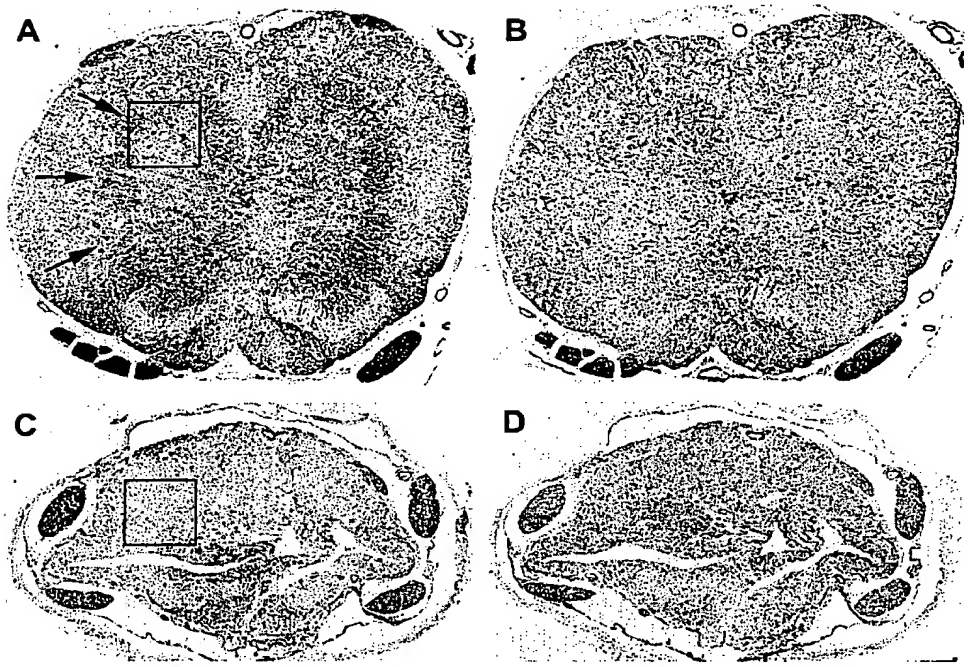

Fig. 8

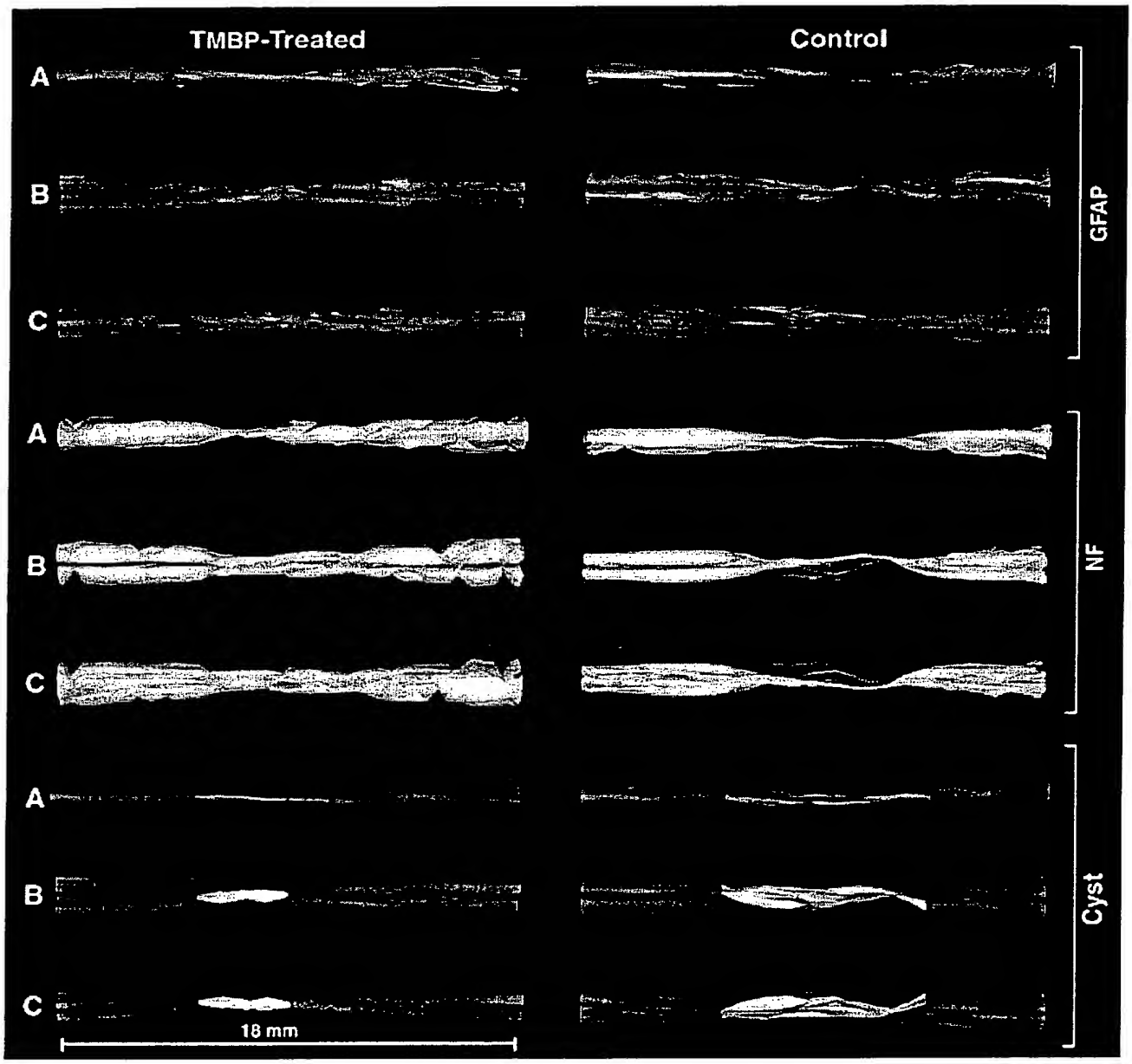

Figure 8. Three-dimensional reconstruction of the spinal cord from serial axial sections stained for GFAP and NF. The spinal injury data consist of stained immunohistological cross sections of spinal cords from T_{MBP}-treated and PBS-treated rats, viewed through a high-resolution scanning confocal microscope. The area in gray outlines the border of the spinal cord. The GFAP-stained area presumably indicates gliosis and scar formation (see Fig. 6). The presence of NFs, shown in green, demonstrates greater preservation of axons in T_{MBP}-treated rats than in control rats. Cyst formation, shown in red, shows that T_{MBP} treatment resulted in a significant (5.2-fold) decrease in cyst volume relative to controls. The cyst volume was calculated and compared by SurfDriver 3.5 software. (**A**) lateral view; (**B**) ventral view; (**C**) dorsal view.

Fig. 9

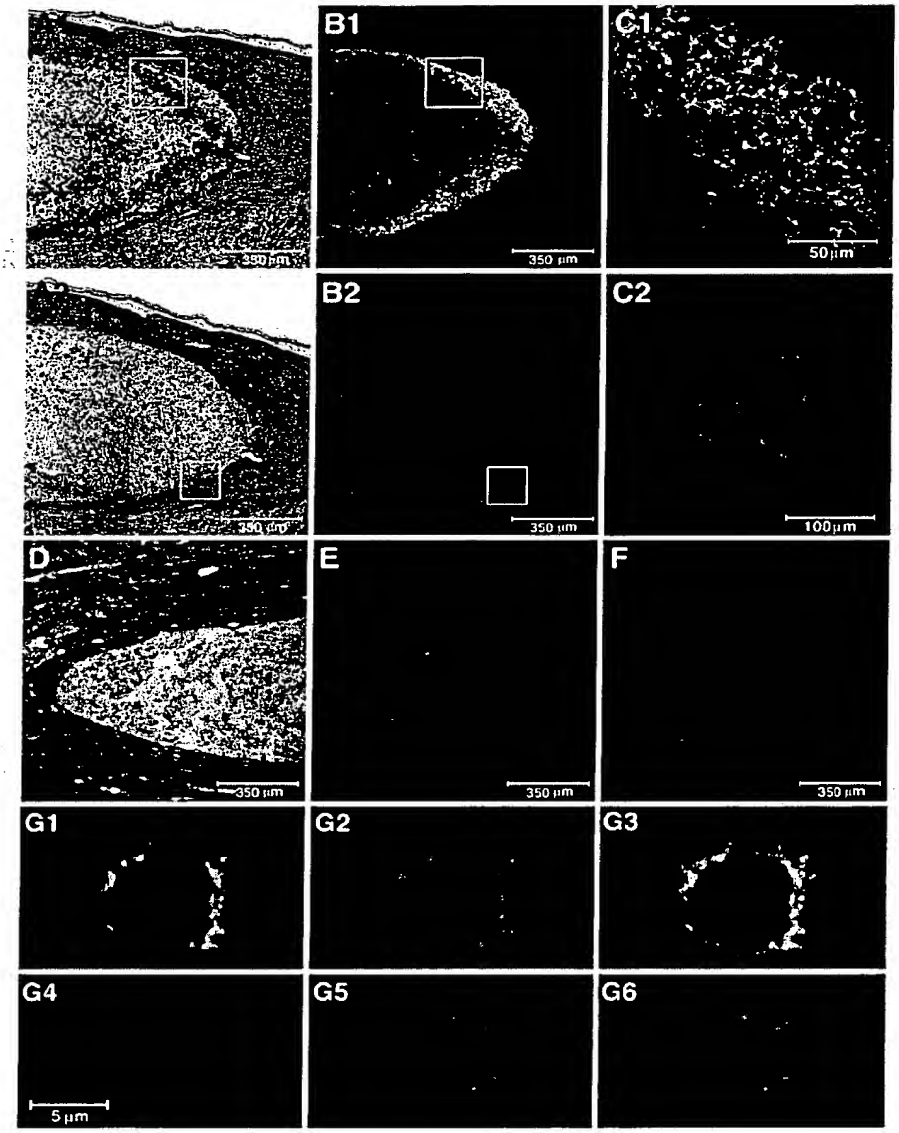

Figure 9. Colocalization of B7-2-expressing cells and T cells on the 14th day after injury in T_{MBP}-treated and PBS-treated rats. Micrographs are from T_{MBP}-treated rats (**A–C**) and PBS-treated controls (**D–F**). Serial longitudinal slices were stained for B7-2 (**A1**) and TCR (**A2**) and analyzed by confocal microscopy. (**A1**) Superimposition of light transmission, on B7-2–labeled cells. Note the B7-2–expressing cells located at the margins of the putative pre-cyst structure. (**B1**) B7-2–expressing cells, same field as in A1, without bright-field. (**C1**) High magnification of boxed area from B1. (**A2**) Same field as in A1, stained for T cells. (**B2**) Same field as in A2 stained for TCR only. (**C2**) High magnification of boxed area from B2. (**D**) Bright-field view of pre-cystlike structures in PBS-treated sections. In contrast to the view seen in A1, there is reorganization of tissue matrix around the pre-cyst-like structure. No staining for B7-2 was detected in this structure (**F**). (**E**) Fewer T cells are seen at the margins of the cystlike structure seen in D. (**G1**) and (**G2**) single-staining for B7-2, TCR, respectively, and (**G3**) double-staining. (**G4–G6**) staining as in (**G1–G3**), except for omitting the B7-2 antibodies. Co-localization of B7-2 costimulatory molecule and TCR at the single-cell level (see Materials and Methods).

Fig. 10

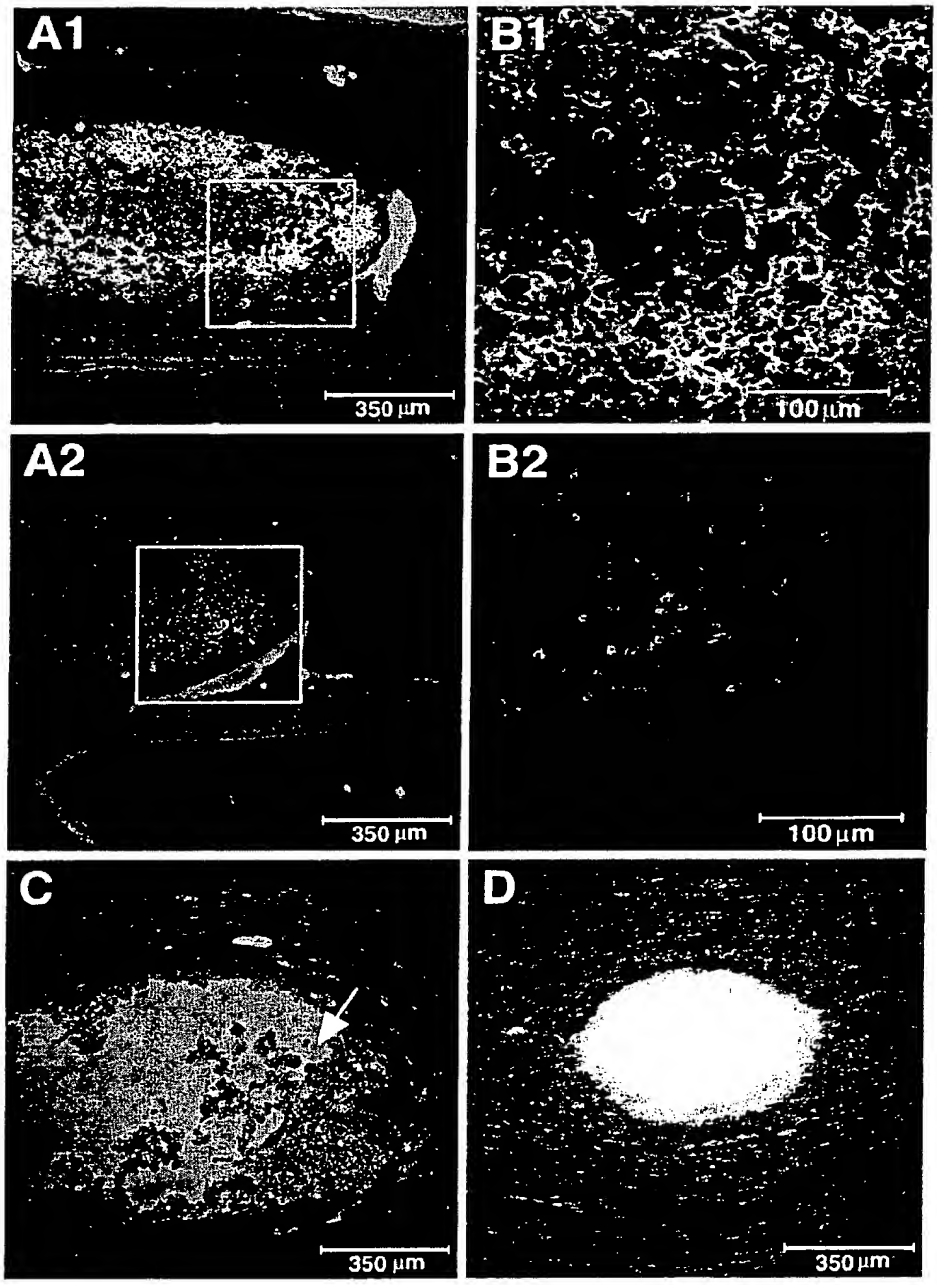

Figure 10. Colocalization of B7-2-expressing cells and T cells on the 28th day after injury in T_{MBP}-treated and PBS-treated rats. Micrographs are from T_{MBP}-treated rats **(A, B)** and PBS-treated controls **(C, D)**. **(A1)** B7-2–expressing cells are present in very large numbers, almost filling the pre-cystlike structure. **(B1)** Boxed area from A1. B7-2–labeled cells only, without bright-field. **(A2)** The same field as in A1, stained for TCR. Note that the cluster of T cells inside the pre-cystlike structure is more condensed than it was 14 days after injury. (Fig. 9, A2). **(B2)** Boxed area in **(A2)** at high magnification. **(C)** Necrotic abrasion, shown by arrow. This section was taken from a PBS-treated cord, at a distance of 6 mm from the site of injury. No staining for B7-2 was detected in this structure. **(D)** A well-formed encapsulated cyst containing no cells. This section was taken at a distance of 8 mm from the site of injury in a PBS-treated control rat.

Fig. 11

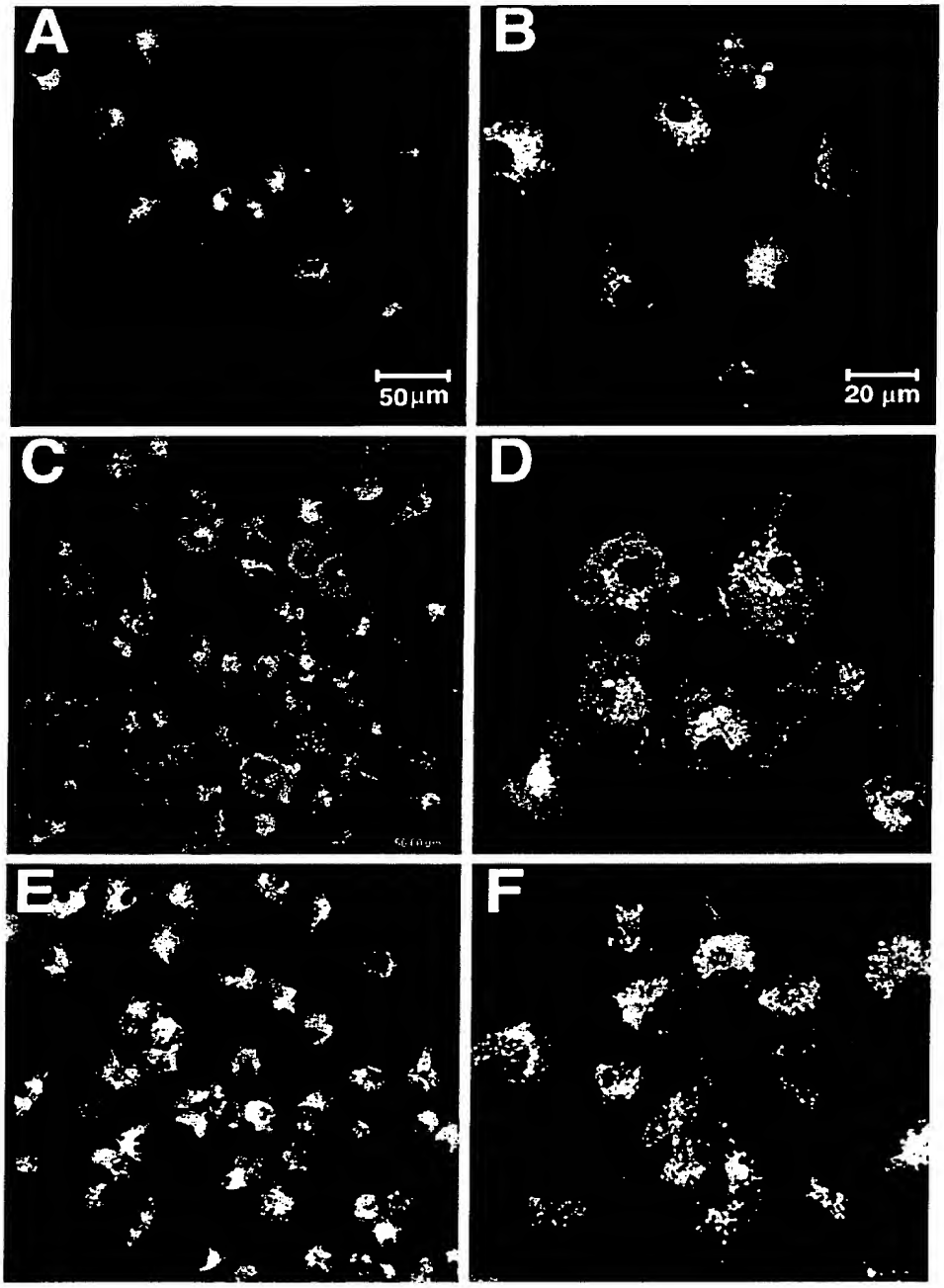

Figure 11. ***In vitro*****, coculturing of primary microglia cells with T_{MBP}-activated cells results in induced expression of B7-2.** Confocal microscopy represents double-staining of microglia cells stained for ED-1 (FITC) and B7-2 (Cy-3). **(A, B)** Control; no T_{MBP} cells were added. **(C,D)** 24 h after co-culturing with T_{MBP} cells ($2x10^3$/well). **(E,F)** – 24 h after co-culturing with T_{MBP} cells (2×10^4/well). (For more details, see Materials and Methods). The data represent results of triplicates from three independent experiments.

Fig. 12

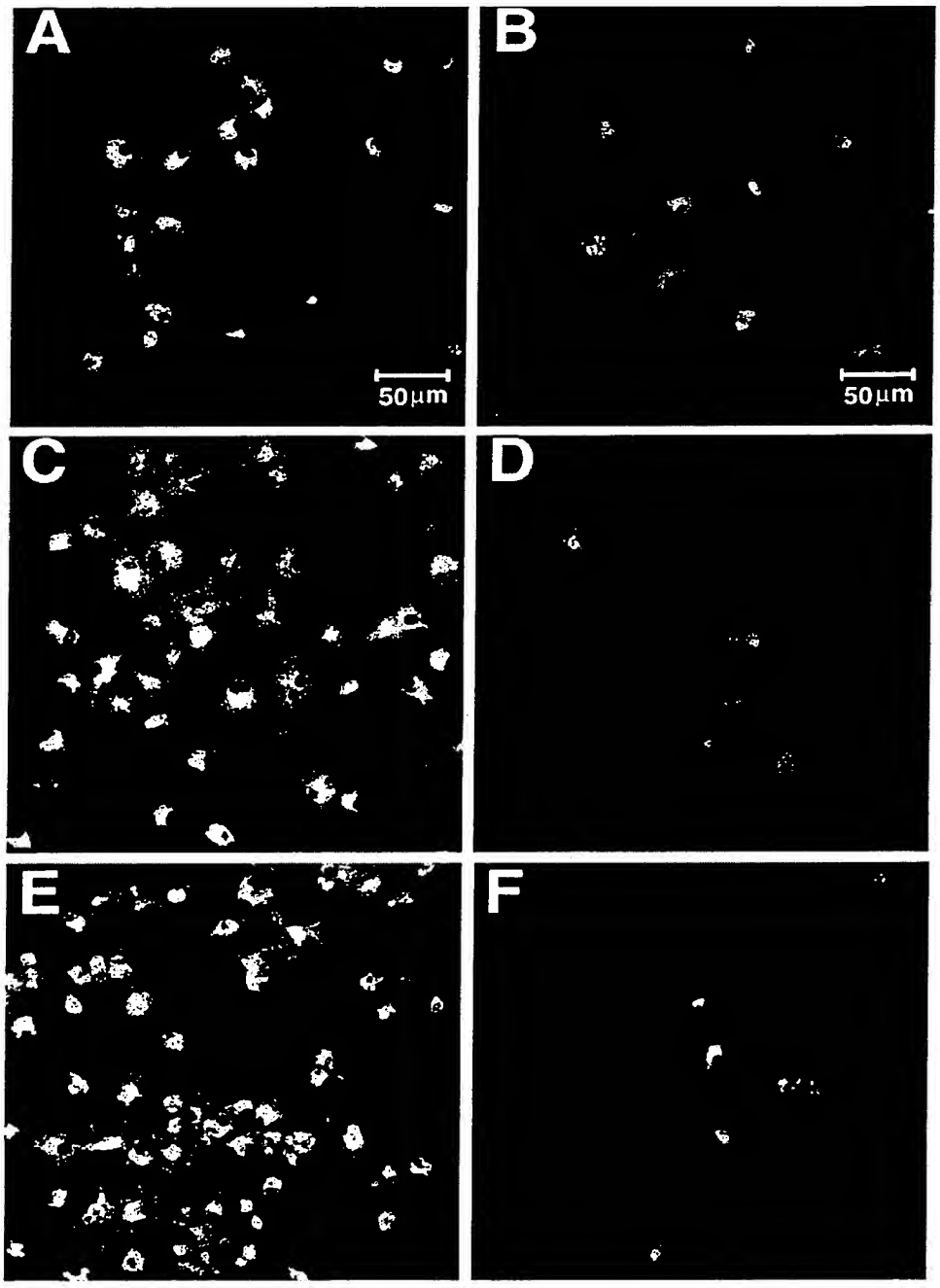

Figure 12. *In vitro* coculturing of primary microglia cells with T_{MBP}-activated cells in the presence of anti-IFN-γ neutralizing antibodies. Effects of anti-IFN-γ antibodies reduce expression of B7-2 and abolish proliferation of microglia. **(B,D,F)** Microglia were treated with 1 μg/ml of anti-IFN-γ antibodies. **(A,B)** No T_{MBP} cells were added. **(C,D)** Twenty-four hours after coculturing with T_{MBP} cells (2×10^3/well). **(E,F)** Twenty-four hours after co-culturing with T_{MBP} cells (2×10^4/well). The experiment was performed in duplicate and repeated two times.

Fig. 13

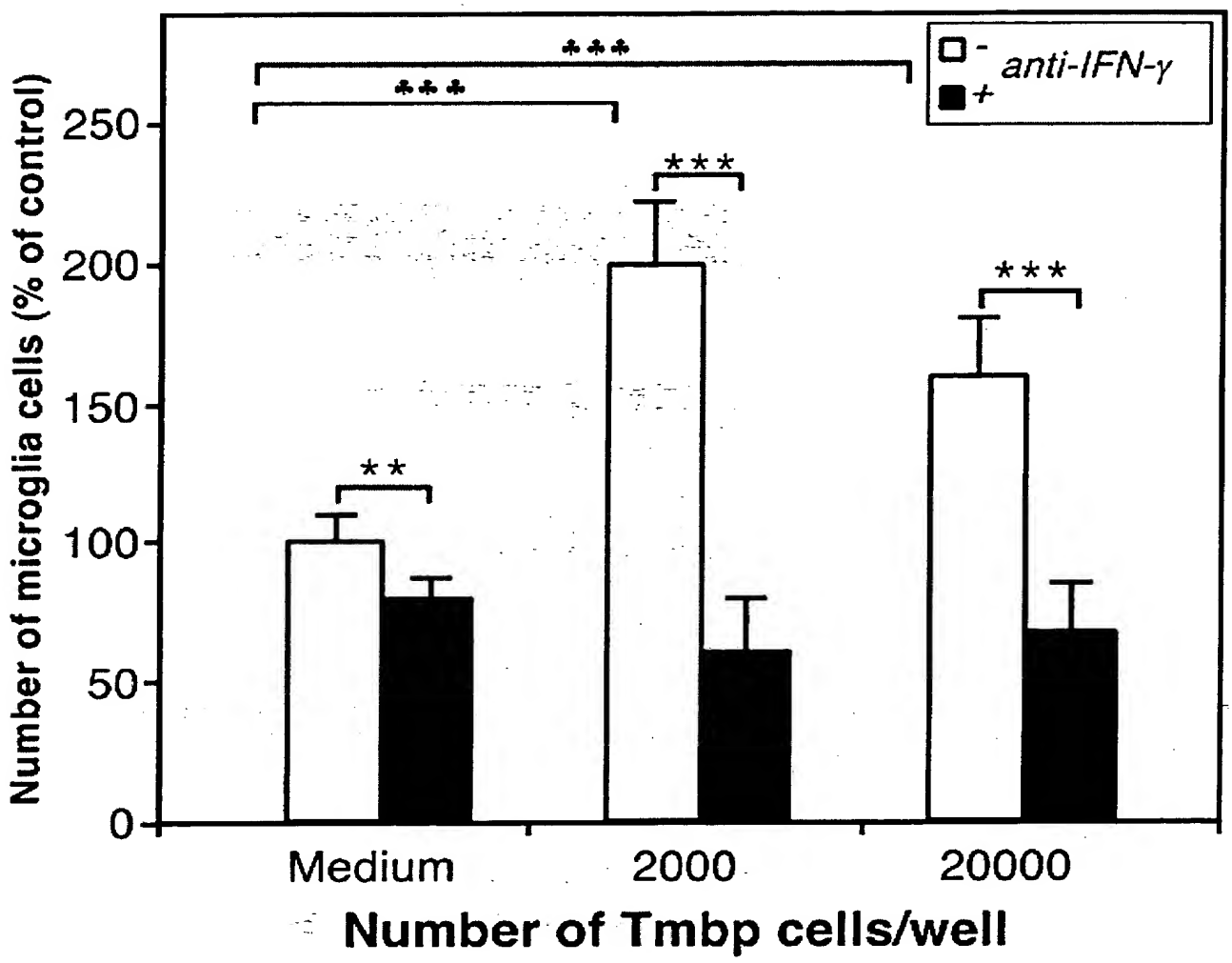

Figure 13. Presence of anti-IFN- neutralizing antibodies inhibits proliferation of microglia cells cocultured with T_{MBP} cells. Statistical analysis (ANOVA) revealed significant differences in the numbers of microglia cells cocultured with T_{MBP} cells in the presence or absence of anti-IFN- antibody ($p<0.001$). The control cells were treated with medium alone. The values are expressed as mean percentage .SD of control when no T cells were added to the microglial cultures (Fig. 12*a*). Microglia treated with T_{MBP} cells alone shows high proliferation relative in microglia cultured in media only ($p<0.001$).